# Design, Transport/Molecular Scale Electronics, Electric Properties, and a Conventional Quantum Study of a New Potential Molecular Switch for Nanoelectronic Devices

Hamid Hadi, Bouzid Gassoumi, Samia Nasr, Reza Safari, A. Aathif Basha, Predhanekar Mohamed Imran, Houcine Ghalla, Maria Teresa Caccamo, and Sahbi Ayachi*

ACCESS | Metrics & More | Article Recommendations | Supporting Information

**ABSTRACT:** In this study, we examined the influence of an external electric field applied in two directions: horizontal ($X$-axis) and vertical ($Y$-axis) on the electronic and vibrational properties of a field-effect molecular switch, denoted as M. We employed density functional theory and quantum theory of atoms in molecules for this analysis. The current−voltage ($I$−$V$) characteristic curve of molecular switch system M was computed by applying the Landauer formula. The results showed that the switching mechanism depends on the direction of the electric field. When the electric field is applied along the $X$-axis and its intensity is around 0.01 au, OFF/ON switching mechanisms occur. By utilizing electronic localization functions and localized-orbital locator topological analysis, we observed significant intramolecular electronic charge transfer "back and forth" in Au−M−Au systems when compared to the isolated system. The noncovalent interaction revealed that the Au−M−Au complex is also stabilized by electrostatic interactions. However, if the electric field is applied along the $Y$-axis, a switching mechanism (OFF/ON) occurs when the electric field intensity reaches 0.008 au. Additionally, the local electronic phenomenological coefficients ($L_{elec}$) of this field-effect molecular switch were determined by using the Onsager phenomenological approach. It can also be predicted that the molecular electrical conductance ($G$) increases as $L_{elec}$ increases. Finally, the electronic and vibrational properties of the proposed models M and Au−M−Au exhibit a powerful switching mechanism that may potentially be employed in a new generation of electronic devices.

## 1. INTRODUCTION

Molecular electronics is one of the most widespread fields of nanotechnology, dealing with the application of molecular building blocks to fabricate electronic components.[1−3] Using this technology, the efficiency of electronic circuits can be increased by miniaturizing electronic components.[4,5] Due to the size effects, as electrical components shrink to nanoscale dimensions (atomic and molecular), the features and quantum properties of these components become more pronounced.[6]

The knowledge of the specific properties of molecular nanoelectronic systems requires the use and knowledge of new codes of quantum mechanics.

Quantum mechanics allows for the study of the electronic−vibrational properties of a nanoelectronic system at the atomic-molecular scale.[7,8] These properties (transport-electronic and vibrational properties) are considered important components in understanding the characteristics of molecular components of the field effect.[9,10] We cite here some of the field-effect molecular components and switches of specific interest.[11,12] Molecular field-effect molecular switches are part of molecular nanoelectronic systems that can switch between two or more states with distinct properties by applying an external electric field (EF).[13,14] In these components, the switching mechanism (ON/OFF) can be controlled by applying an external EF.[15,16] In fact, the external EF causes electron transfer (ET) and changes in the electronic properties of these components (mainly conductivity).[17,18] In this context, the control of ET is very important. For instance, various models and methods have recently been

employed to describe molecular nanoelectronic devices or systems using experimental or semiempirical data.[1,19−22] In this study, we investigate the external field's effect on the switching mechanism (ON/OFF) of a candidate molecular switch, as depicted in Figure 1. We conduct this analysis using density functional theory (DFT) and quantum theory of atoms in molecules (QTAIM), applying a quantum method and model without reliance on experimental data.

Among the important points in this research was the purposeful design of a field-effect molecular switch with acceptable performance. In this regard, based on preliminary theoretical−computational predictions (and performing semi-experimental evaluations and preliminary calculations on several suggested molecular structures), a molecular switch with the ability to switch due to the application of an external EF was finally proposed. This studied molecular switch, which belongs to the family of conjugated anthracenes (Figure 1), is predicted to exhibit a wide range of desirable properties, including:

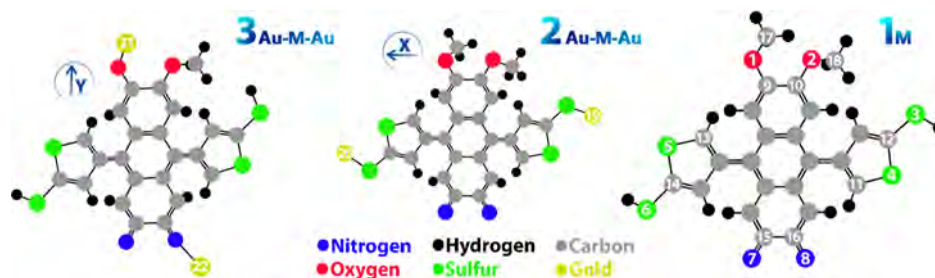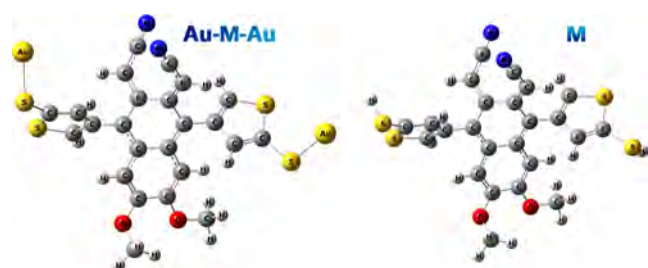- Ability to connect to electrodes (as shown in Figures 1 and 3).

**Figure 1.** Molecular switch is applied to the EF (along the *X*- and *Y*-axes). M: isolated system; Au−M−Au: nonisolated one.



**Figure 2.** External EF intensity applied (along the *X/Y*-axes): low (LB), threshold (TB), and high (HB) applied field intensity range (ON/OFF).



**Figure 3.** Optimization structure of the molecular switch studied in this work in the isolated (M) and nonisolated (Au−M−Au) states.

- The ability to achieve an optimal electronic structure under the influence of applied fields (as shown in Figure 3).
- A relatively small energy gap exists between the frontier molecular orbitals (HOMO/LUMO) (as shown in Figure 8).
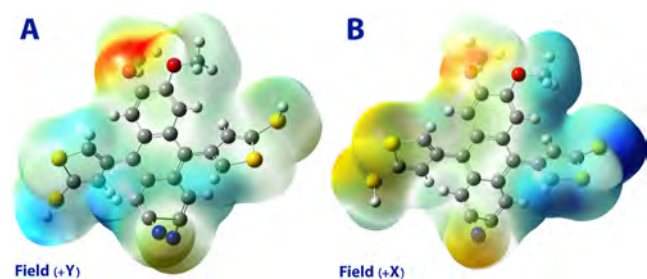


**Figure 4.** Electrostatic potential map (MEP) of an isolated molecular switch (M) (along the *X*- and *Y*-axes).

- Observable and measurable electronic/vibrational responses to applied fields (as shown in Figures 8−10).
- Acceptable electrical conductivity (as shown in Figure 15).
- Field-effect switching capability (as shown in Figures 15 and 16).
- Expansion of unstable π-bonds along the molecule's length and in the direction of the applied field (as shown in Figure 16).
- Resonance capability (as shown in Figures 16 and 17).

- Suitable intramolecular partitioning capability (as shown in Figure 17).
- Cost-effective synthesis.
- Acceptable chemical and physical stability, particularly at low temperatures.[23]
- Nontoxicity from a green chemistry perspective.[24]

We studied the external EF's effect on both the isolated state of M (before connecting to the electrode) and the nonisolated state of Au−M−Au (after connecting to gold metal electrodes) in the molecular switch shown in Figure 1.

In this context, the local electronic intramolecular phenomenological coefficients and the current−voltage (*I*−*V*) diagram are based on the Onsager's phenomenological approach to this molecular switch in M and Au−M−Au states using Landauer and topological (QTAIM) theories.

## 2. QUANTUM COMPUTATIONAL DETAILS

DFT/CAM-B3LYP/6-311+G(d,p) calculations were performed for the optimization of molecular geometry and studied the effects of the EF on the structural and vibrational as well as electronic properties of isolated molecular switches (M) and nonisolated (Au−M−Au). The hybrid exchange-correlation functional CAM-B3LYP is very suitable for this study based on its good performance in predicting molecular geometry parameters and energy. Accurately predicting electric properties is generally a more difficult task for CAM-B3LYP.[25] For the gold atoms (electrodes), the LANL2DZ[26] pseudopotential was used.

Vibration frequency and cohesive energy (eq 1) were studied as two important parameters to confirm the feasibility of forming the designed molecular structures.

$$E_{\text{Coh}} = -\left(E_{\text{tot}} - \sum_i n_i E_i\right)/n \tag{1}$$

where $E_{\text{tot}}$, $E_i$, and $n_i$ are the total energy of all designed molecules, the atomic energy, and the number of atoms, respectively, and $n$ is the total number of all atoms.[27] The important factor that determines the intrinsic properties of all types of molecules is the position of the conduction and valence bands and the gap between them. The density of electronic state (DOS) and energy gap (eq 2) were computed to predict the electronic properties of the designed structures using the GaussSum03 software.[28]
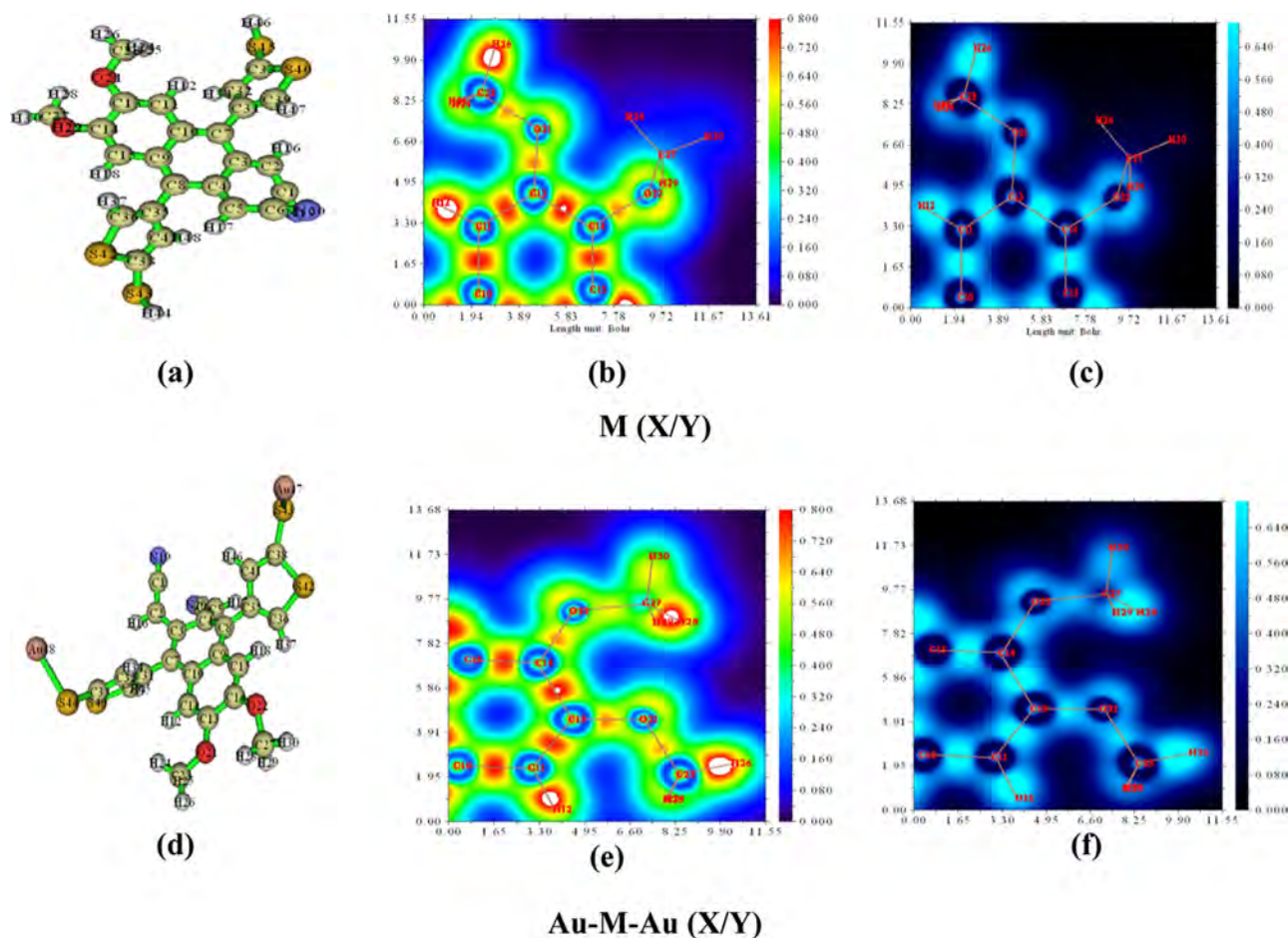
**Figure 5.** LOL maps of the isolated system (M) and molecular switch (E−M−) (along the $X/Y$-axes).
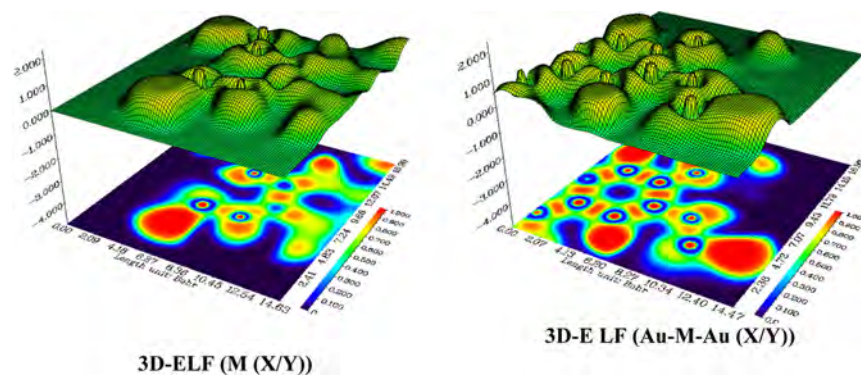


**Figure 6.** ELF maps of the isolated system (M) and molecular switch (Au−M−Au) (along the $X/Y$-axes).

$$HLG = |E_{LUMO} - E_{HOMO}| \qquad (2)$$

$E_{HOMO}$ represents the energy level of the highest occupied molecular orbital (HOMO), and $E_{LUMO}$ signifies the energy level of the lowest unoccupied molecular orbital (LUMO).[29]

Furthermore, Landauer's formula (eq 3) was used to predict the diagram of the current−voltage ($I−V$) curve of the studied models.

$$I = \frac{2e}{\hbar} \int T(E; V)[f(E - \mu_L)] - [f((E - \mu_R))] \, dE \qquad (3)$$

where $e$ is the electron charge, $\hbar$ is Planck's constant, $T(E, V)$ is the ET coefficient due to the bias voltage effect ($V$), and $f(E - \mu_L, E - \mu_R)$ denotes the Fermi−Dirac distribution function for electrochemical potential ($\mu_L, \mu_R$) for left and right electrodes.[30] Furthermore, the temperature-independent direct tunneling electric conduction ($G$) was determined using the Landauer formula in single-molecule nanoelectronic systems; the expression is as follows

$$G = \frac{1}{R} = \frac{2e^2 \tau_e}{\hbar} \qquad (4)$$

$$\tau = \exp(-\beta L) \qquad (5)$$

$$\beta = \left(\frac{2m^* \alpha \varphi}{\hbar^2}\right)^{1/2} \qquad (6)$$
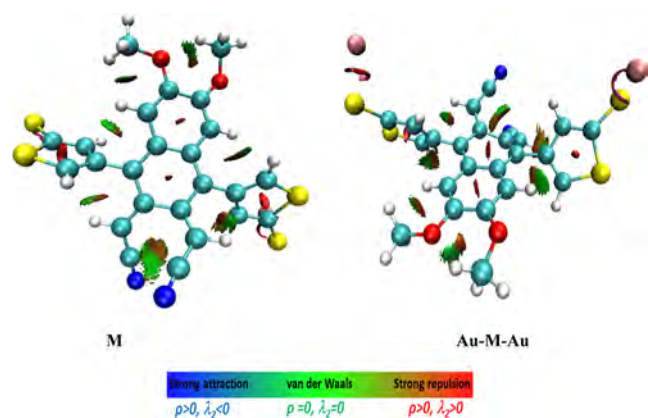
**Figure 7.** NCI index maps of the studied compound.

where $\hbar$ is $\frac{h}{2\pi}$ and $\varphi$ is the height potential barrier for tunneling through the HOMO or the LUMO level, which is equivalent to the energy difference between the Fermi energy and the molecular HOMO or LUMO level. $m^*$ is the effective mass of the electron ($m^* = 0.16\ m_0$, with $m_0$ being the free electron mass). $\alpha$ is the symmetry parameter in the potential profile; in this symmetric case, $\alpha = 1$.[31]

As the potential barrier $\varphi$ plays an important role in the ET mechanism in molecular components, we have represented three ranges of applied field intensity (along the X- and Y-axes) in our studied molecular switching systems.

(1) The low field intensity, LB ($\varphi >$ EF); (2) the threshold field intensity, TB ($\varphi \approx$ EF); and (3) the high field intensity, HB ($\varphi <$ EF), ($\varphi$ and EF (eV), see Figure 2).

## 3. RESULTS AND DISCUSSION

**3.1. Molecular Switch Optimization.** The designed molecular switch structure was optimized at the DFT/CAM-B3LYP/6-311+G(d,p) level of theory. To ensure convergence, the vibrational modes were computed with the same level of theory, and no imaginary frequency has been found. The values of the cohesive energy are calculated using eq 1 and found to be 154.73 and 176.24 kcal·mol$^{-1}$ for M and Au−M−Au,

respectively. The optimized structures of M and Au−M−Au are depicted in Figure 3.

**3.2. MEP Analysis.** Molecular electrostatic potential (MEP) maps serve as valuable tools in molecular modeling, allowing for the comprehension of molecules' electrostatic properties and the prediction of their behavior.[32−35] These maps can guide experimental research and offer insights into chemical reactions. However, it is important to note that they represent theoretical predictions rather than direct confirmations of experimental results, which depend on physical measurements and observations.

If an MEP map indicates that a specific region of a molecule is electron-rich and likely to participate in a chemical reaction and subsequent experimental data validate such reactivity at that location, it can lend support to a computational model. MEPs are commonly employed in the form of reactivity maps that highlight probable sites for electrophile (electrode) binding on organic molecules.[36] This is a fundamental aspect of molecular modeling research. The MEP map is generated by using the DFT/CAM-B3LYP/6-311+G (d,p) method, and the maps are presented in Figure 4.

The MEP surface color scheme is as follows: red represents a partially negative charge; blue represents a partially positive charge and a deficiency of electrons; light blue represents a slightly electron-deficient region; yellow represents a slightly electron-rich region; and green represents a neutral region.[37] The blue and red regions indicate the electropositive and electronegative regions, respectively. The region of red (electron-rich) is located around the nitrogen and oxygen atoms, where electrophilic attack is possible. The yellow region (electron-poor) is spread all over the molecule around hydrogen and carbon atoms, which is prone to nucleophilic attack.[38]

It is clear that along the X- and Y-axes, oxygen, nitrogen, and sulfur atoms are surrounded by negative electrostatic potentials, and the ESP around these atoms is more extended than that around other atoms in space. This is due to the high electronegativity of these atoms. Therefore, it seems that the atomic basins of sulfur, oxygen, and nitrogen are the active places of charge/energy exchange and the places of connection of electrodes in the molecular switch.
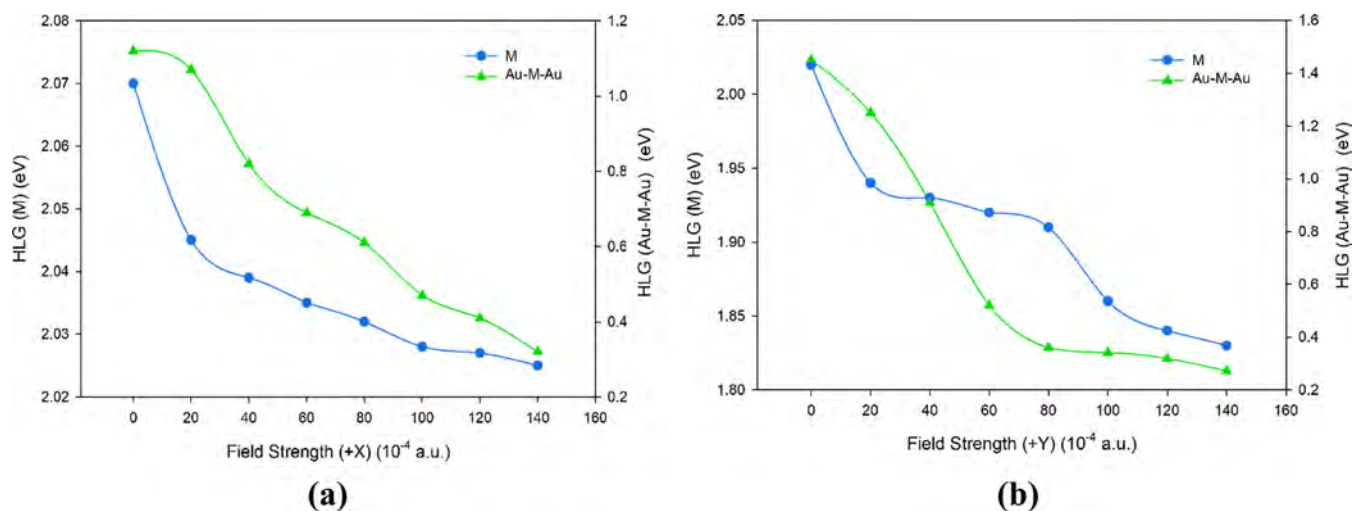


**Figure 8.** Effect of the EF on the energy gap in the designed models, with (a) representing M and (b) representing Au−M−Au along the X- and Y-axes, respectively.
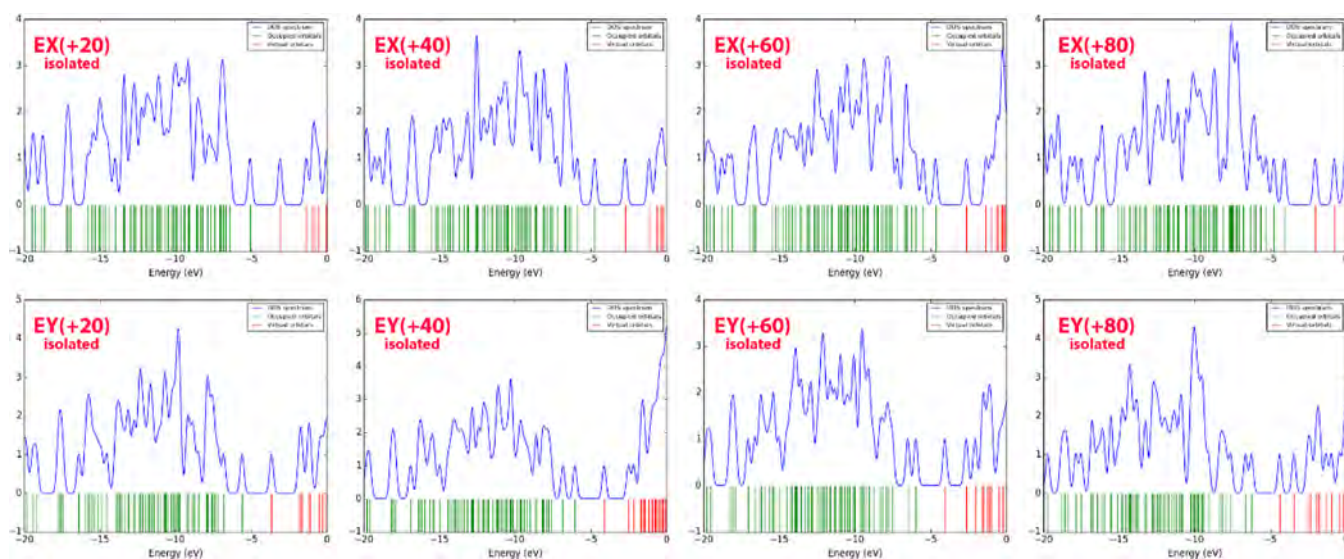
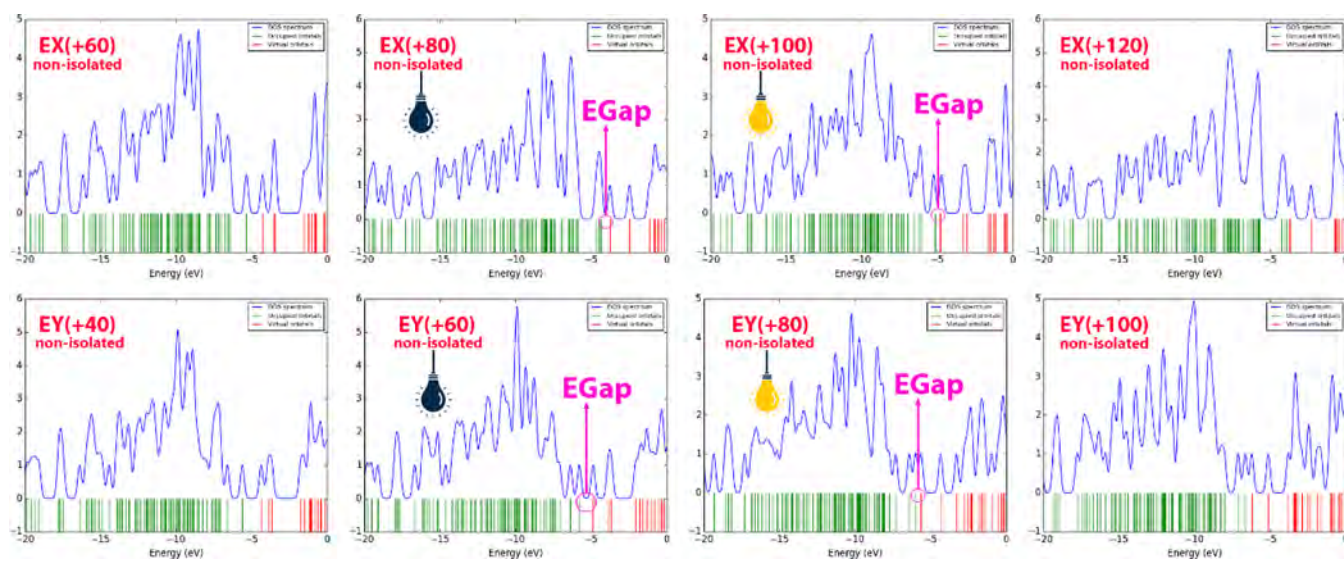**Figure 9.** Electronic DOS of the isolated system (M).



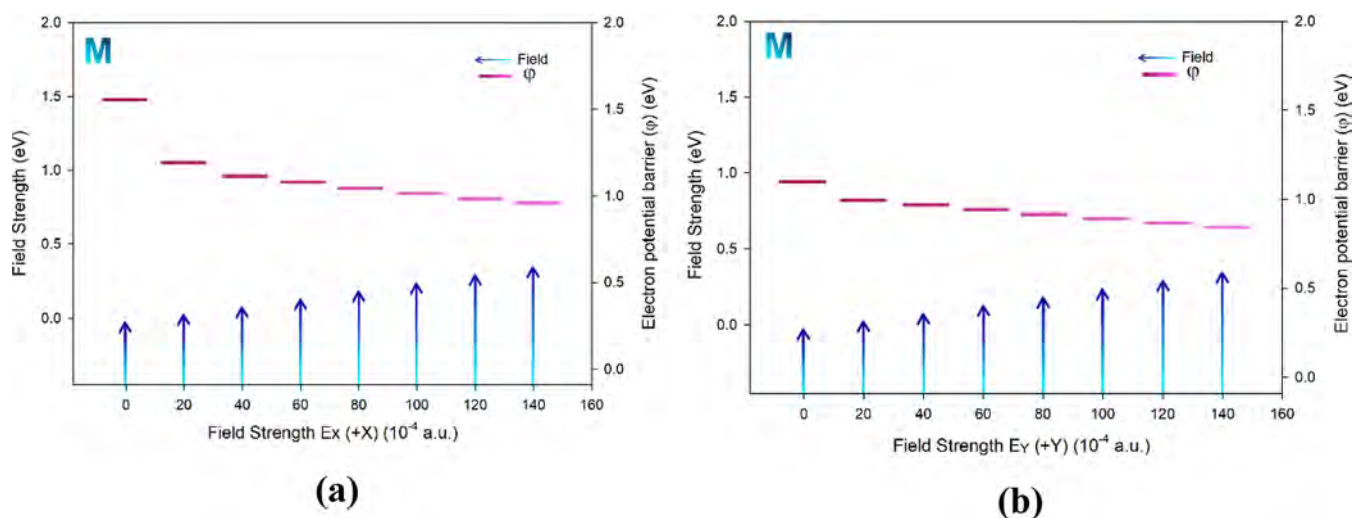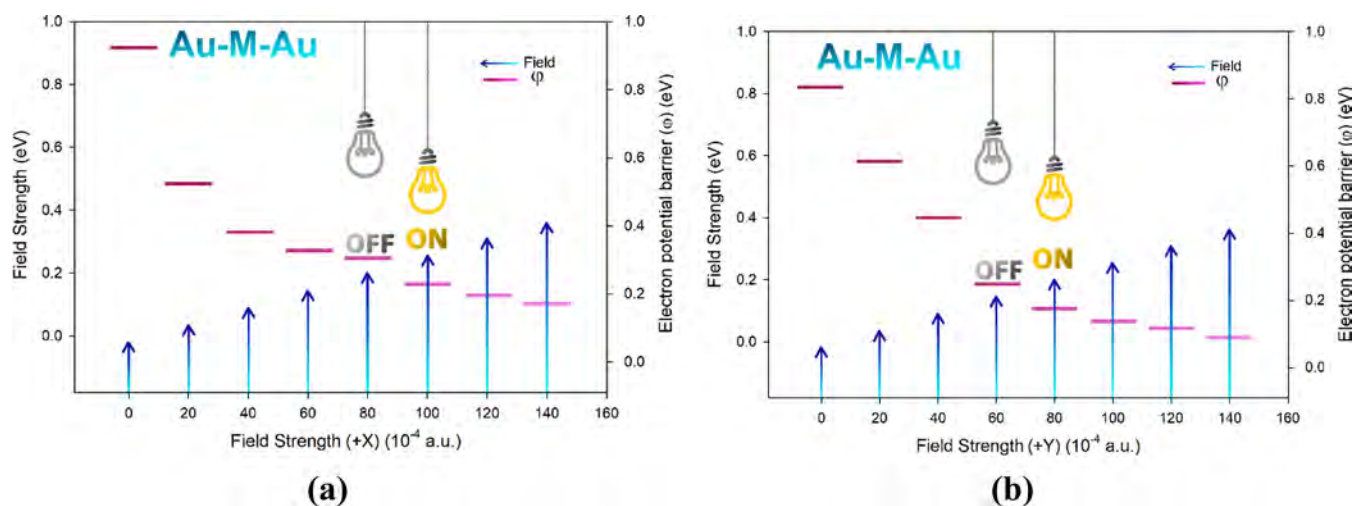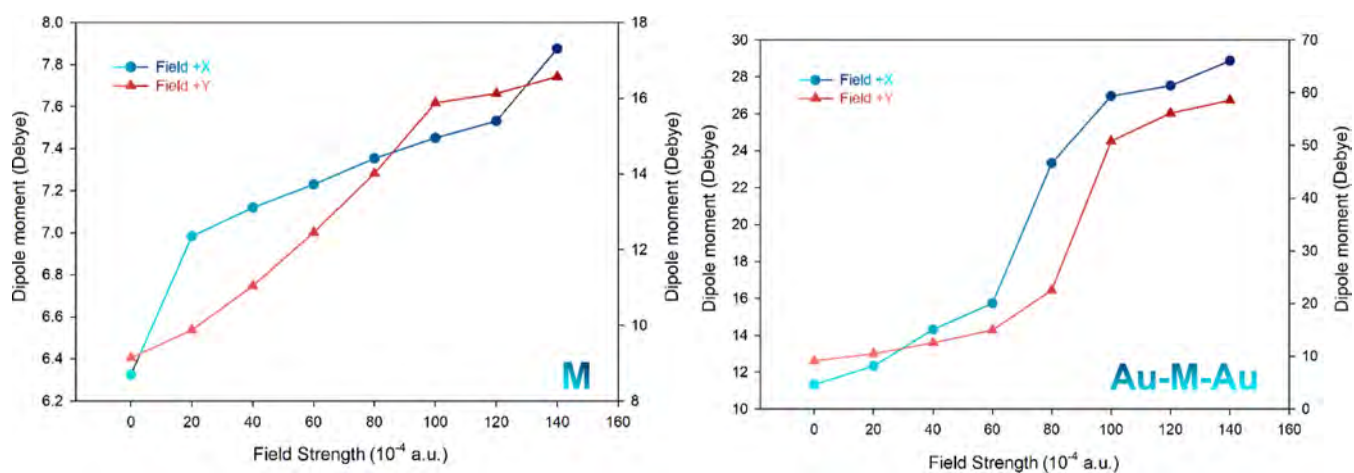**Figure 10.** Electronic DOS of the nonisolated system (Au−M−Au).



**Figure 11.** Effect of applying an EF [(a,b): M along the *X*- and *Y*-axes] on a designed molecular switch in an isolated state (M).

**Figure 12.** Effect of applying an EF [(a,b): M along the *X*- and *Y*-axes] on a designed molecular switch in a nonisolated system (Au−M−Au).



**Figure 13.** Effect of the EF (along the *X*/*Y*-axes) on the dipole moment of the proposed molecular switches.
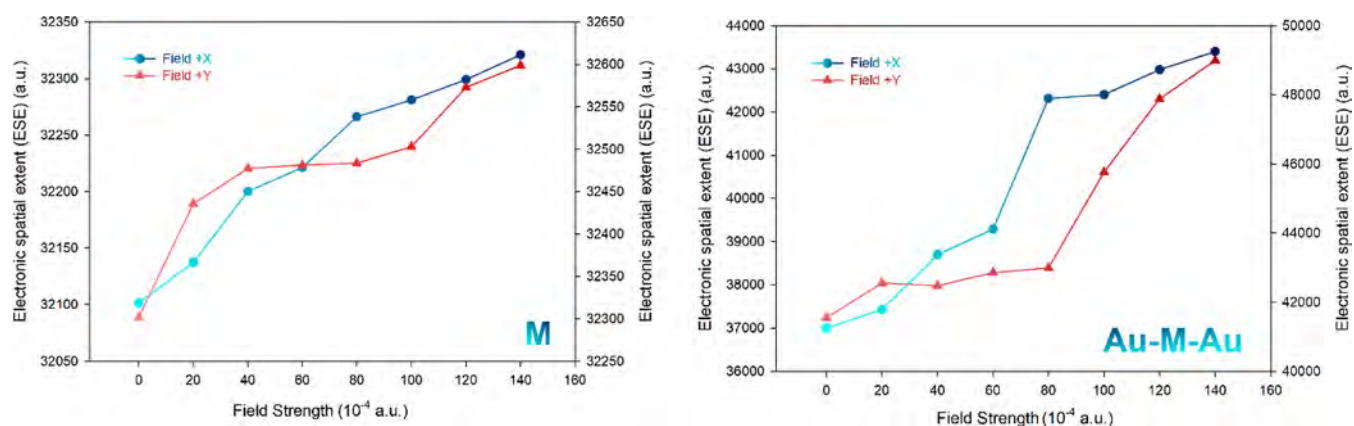


**Figure 14.** Effect of the EF (along the *X*/*Y*-axes) on the ESE of the proposed molecular switches.

**3.3. Localized-Orbital Locator Analysis.** The proposed localized-orbital locator (LOL), chemically coded by Selvin and Savin,[39] is beneficial to describe the major electronic concentrations on the surface of our studied compounds. It is preferable to demonstrate the location of free electrons on surfaces, which facilitates the charge transfer phenomena between chemical groups.[40−43] Figure 5 displays the M material,

the Au−M−Au system with atomic numbering, and the 2D-LOL figures along the *X*- and *Y*-axes.

It is shown that there are appearances of red spots surrounded by yellow, which deduces the existence of the delocalization path of the π electron. It clearly appears that the π-benzene ring part of the M molecule is chromatized by the strong electronic delocalization effect (red-yellow), and the $C_{13}-O_{21}-C_{23}$ and $C_{14}-O_{22}-C_{22}$ groups appear to contain minor delocalized
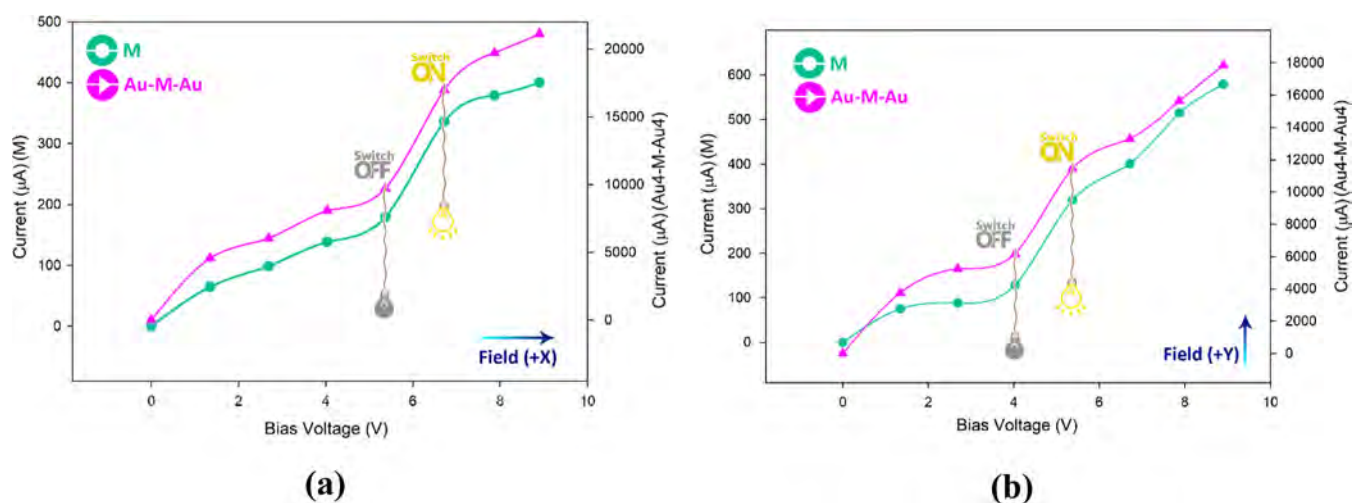
**Figure 15.** I−V curve in M and Au−M−Au states: (a) applying the field along the Y-axis and (b) applying the field along the X-axis.
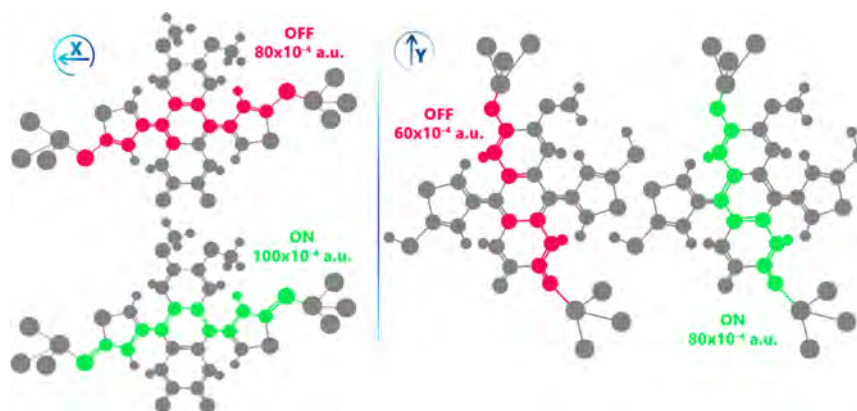


**Figure 16.** ON and OFF switching mechanisms of the studied molecular system.
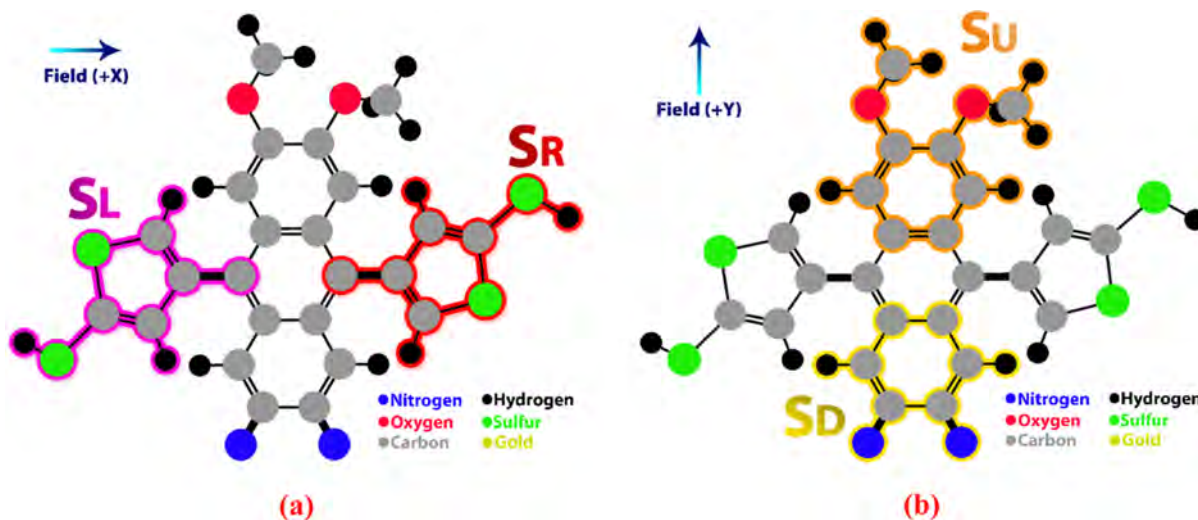


**Figure 17.** Intramolecular sections (S$_L$;S$_R$) (S$_U$;S$_D$) of the molecular switch M [(a) along the X-axis and (b) along the Y-axis].

electronic contributions (Figure 5b). As can be seen from Figure 5c, the M compound reflects this phenomenon by exhibiting a major delocalization of the π electron on the surface of the ring and a minor one in the other extremity groups. These findings concluded that the high charge activity on the surface signifies the existence of charge transfer phenomena on the surface of our compound. In addition, concerning the switch molecule Au−

M−Au, it is found that the existence of the delocalization effect is increased in the aromatic ring (red-yellow) and highly (red) appears in the groups of H28−C27−H30 and H23−C23−H26 (Figure 5e). The presence of highly charged sites on the surface of the switch molecule, in contrast to the isolated compound, is a result of the sandwich effect with metal Au. Therefore, the interactions of the nonbonding pairs in the valence shell of Au

with the molecule disturb the charge activity properties and enrich the efficacy of charge transfer between Au, M, and Au. This idea is well confirmed by 2D-LOL Figure 5f, where it is shown that the black and white colors that justify the existence of the delocalized π-electron are highly visible almost on all surfaces of our system. This idea confirms the high charge transfer that occurs in the switch molecule in comparison to that in the isolated one. Finally, it is deduced that the lone electron pairs of the oxygen atoms with the atoms yielded by the metal make our system energetically charged; therefore, it is a powerful model to be present in the environment as a molecular switch.

**3.4. ELF Analyses.** The 3D-dimensional electron localization function (ELF) is a powerful method used to measure the probability of coexisting electrons in proximity space. The explanation of this quantum theory is deeply discussed by Becke and Edgecombe in their literature overview.[44,45] The theory of ELF analysis is based on the following script

$$\text{ELF}(r) = \frac{1}{1 + (D(r)/D_0(r))} \qquad (7)$$

where

$$D(r) = 1/2 \sum_i^\eta i|\nabla_i| - \frac{1}{8}\left[\left\|\left\|\frac{\nabla\rho\alpha(r)}{\rho\alpha(r)}\right\|\right\|^2 + \left\|\left\|\frac{\nabla\rho\beta(r)}{\rho\beta(r)}\right\|\right\|\right] \qquad (8)$$

$$D_0(r) = 3/10(6\pi^2)^{2/3}[\rho_\alpha(r)^{5/3} + \rho_\beta(r)^{5/3}] \qquad (9)$$

$\rho_\alpha(r)$: electron density of spin $\alpha$, and its Laplacian $\nabla\rho\alpha(r)^2$; $\rho_\beta(r)$: electron density of spin $\beta$, and its Laplacian $\nabla\rho\beta(r)^2$

Herein, we have concentrated on the localization of the spin-electronic contribution on the surface of our complex for demonstrating that energy and charge transfer occur highly in the surface area of the compound after the addition of metal Au. The 3D-ELF [M and Au−M−Au $(x/y)$] maps are depicted in Figure 6. In comparison between the isolated molecule and the switched one, in Au−M−Au, it is observed that a high degree (red) of localization of spin-electronic concentrations has been witnessed between the aromatic ring and the other extremity, where there is the location of oxygen, sulfur, and nitrogen. The ELF value appears to be relatively high, possibly reaching 1 atomic unit.

This value is rarely obtained for organic complexes, which proves that there is a back and forth flow of impeccable numbers of electrons at the surface level; therefore, there is a rather high charge transfer detected during the addition of Au metals. In addition, it is noted that the electronic accumulation of double-spin electrons is in excess in the atomic basin of oxygen and sulfur. Therefore, the nonbonding of the valence shell of these atoms favors a transfer of intramolecular charge trapped between the groups that are attacked by the silver, so it can be deduced that these places are suitable for the installation of gold electrodes. Thus, our molecule acts as an interrupter system in electronic devices.

**3.5. Noncovalent Interaction Analysis.** The noncovalent interaction (NCI) index is an extension of QTAIM topological analyses elaborated by Bader.[46,47] This powerful approach has been widely employed to identify in color code the types of interactions, for example, hydrogen, van der Waals, steric effects, and π−π stacking binding strengths. It is beneficial to demonstrate the production of charge transfer reactions between atoms in the studied compounds. In addition, the NCI theory is applied to confirm the presence of electronic

exchange between the donor and acceptor systems.[48−52] The 3D-NCI plots are depicted in Figure 7. Concerning the M material, it appears that the green spots between the hydrogen atoms and the π-aromatic groups and between the hydrogen and the oxygen atoms evolved from the existence of charge rearrangement at the surface level, which deduces that the molecule is actively charged and stabilized by electrostatic interactions. Therefore, there is a charge transfer phenomenon taking place at the surface level. The molecule switch also presents localized green spots between the H atoms and the π-aromatic benzene group, indicating that the complex is also stabilized by van der Waals-type interactions. Therefore, there is electronic accumulation at the surface level of the molecule, which forces the appearance of these types of forces. The steric spots between the Au metal and the sulfur atom deduce the increase in the energy of the molecule in this region. Physically deep, Au cations interacting with sulfur in both areas appeared as a boiling repellent wall of electrons. Therefore, the switch molecule is much more active and can be utilized as an interrupter molecule in a new electronic technology.

**3.6. QTAIM Analysis.** To determine the optimal location for installing gold electrodes, we investigated the impact of the external EF along the $X$- and $Y$-axes (as shown in Figure S1a,b) on the isolated molecular switch.

For this purpose, the structure of the molecular switch was optimized by the use of the DFT/CAM-B3LYP/6-311+G (d,p) theoretical level and sited in the EF intensity of $0−140\cdot(10^{-4}$ au) along the $X$- and $Y$-axes. Then, the local response of each atom to the applied external EF was investigated using the QTAIM theory.

If we interpret the effect of the field applied along the $X$-axis on the atomic basins (Figure S1a), the analysis of the topological results of QTAIM shows that the sulfur atomic basins are the most important in comparison with the other atomic basins. Moreover, when the EF is applied along the $Y$-axis (Figure S1b), the oxygen and nitrogen atomic domains show the greatest reaction to the applied field (Figures S1 and S2). According to the findings presented in this study, the molecular switch (M) can be categorized into sections that function as intramolecular acceptors or donors (termed n-like or p-like, respectively). As a result, it is feasible to ascertain the specific contribution of each individual intramolecular section (or atomic basin) to the process of intramolecular charge and energy transfer. According to the obtained results, it is expected that nitrogen, oxygen, and sulfur atomic basins are suitable places for installing gold electrodes. The results obtained from MPE and QTAIM for different atomic basins had a good overlap with each other.

**3.7. Structural Properties (Length Changes).** In this study, we measured the EF intensity in volts per unit length ($\varepsilon = V/l$). Here, $l$ represents the length of the molecular device, which is the distance between the two poles or terminals of the circuit, each belonging to one part of the molecule. We express this measurement in atomic units (1 au = 514.224 V/nm) throughout this work. To maintain the structural integrity of the molecular switch, we applied fields with a relatively low intensity. Consequently, we anticipate that the structural changes resulting from this range of applied field intensities will be moderate and not overly severe.

As an additional result, in the models M and Au−M−Au, it is concluded that by increasing the intensity of the applied EF, the variation of the interplane angles in all molecular systems increases, while on the other hand, the planarity of these systems decreases slightly (see Figure S4a,b).

According to the results we obtained, there is a minor decrease in the length of the molecular structure in both the isolated (M) and nonisolated (Au−M−Au) states as the applied field intensity increases (as shown in Figures S3 and S4).

Reducing the length of the molecule is related to reducing the bond length between atoms. The bond length changes in response to field application for some important atoms (in the isolated state) are given in Figure S4a,b. When the EF is applied in the direction of the X-axis, the most changes occur in the bonds related to atoms S6−C14 and S3−C12. This is despite the fact that by applying an EF in the direction of the Y-axis, the bonds between atoms O2−C10, O1−C9, N7−C15, and N8−C16 show the greatest reaction to the applied field.

**3.8. Electronic Properties and DOS Spectra.** The frontier HOMO orbitals give information about the valence band, and the frontier LUMO orbitals give information about the conduction band of the molecules.[53] The reduced energy band gap ($\Delta_{H-L}$) indicates the shortening of the potential barrier for the passage of electrons, which affects the performance of a nanoelectronic system.[54] In addition, to show the importance of molecular orbitals in chemical bonds, we used DOS diagrams. The DOS diagram shows an overlapping population of molecular orbitals as well as the orbital group composition of the molecular orbital.[55] In this section, the effect of the EF (along the X/Y-axes) on the frontier orbitals (LUMO/ HOMO) and the band gap between them (HLG) in isolated (M) and nonisolated (Au−M−Au) states was investigated. The calculated energies of the frontier molecular orbitals (FMOs) ($\varepsilon_{HOMO}$ and $\varepsilon_{LUMO}$), the energy band gap difference, and the DOS spectra are illustrated in Figure 8.

In Figure 8a,b, it is noted that the HOMO−LUMO gap (HLG) of our first model depends on the applied field intensity. This result indicates the effectiveness of our molecular switch's response to applied field properties, such as the direction of field intensity. It is concluded that the observable and measurable response of our systems is in conjunction with the properties of the applied field. Under the effect of an applied external field, it causes molecular electronic (atomic) changes that coexist with an increase in the distribution (redistribution) of charge and energy transfer in parallel and perpendicular directions between different atomic basins (the different intramolecular sections).

Furthermore, we conducted an investigation into the effect of the EF on the molecular DOS for both the M and Au−M−Au switches, as depicted in Figures 9 and 10. The DOS refers to the number of distinct states at a specific energy level available for electrons to occupy or the number of electron states per unit volume per unit energy. This fundamental concept is used to explain and rationalize the existence of the energy gap in the electronic band structure of a material. The DOS provides valuable insights into the involvement of HOMO−LUMO frontier orbitals and, consequently, the reactivity of the system.

In addition, in Figures 9 and 10, it is clearly observed that the effect of the EF on the electronic DOS of our proposed molecular switch is that the electron density depends in an almost nonlinear manner on the effect of the increase in the intensity of the EF.

**3.9. Electron Barrier Potential.** As can be seen from Figures 11 and 12a,b, the switching mechanism of this molecular switch in the x direction is completely different from the y direction. It seems that the cause of this difference is the difference in the mechanism of expansion of an unstable $\pi$-conjugated system in the x and y directions. In addition, as can be seen from these figures, the spatial expansion and energy of

boundary molecular orbitals are noticeably dependent on the intensity (and direction) of the applied field. Furthermore, applying an external EF along the X-axis not only alters the charge distribution mechanism and spatial expansion of the frontier molecular orbitals of this molecular switch in the x direction but also affects these properties in the y direction.

**3.10. Dipole Moment and Electron Spatial Extent.** Atomic basins and atomic displacement vector moments (certain electronic and vibrational properties of the system) change under the external EF effect applied to a molecular system as a measure of the field response. For this purpose, in the M and Au−M−Au models, we have investigated the molecular dipole moment tensors and vectors as an index measuring the response to the external EF (see Figure 13).

The electronic responses to the effects of external EF on molecular systems are explained by the separation of the corresponding electron densities, meaning the separation of negative and positive charge centers in our models. This characteristic is influenced by the change in the dipole moment in our models. Also, for the M and Au−M−Au systems, the EF effect on molecular dipole moment tensors ($\mu i$) was calculated. As shown in Figure 13, the ($\mu i$) varies in a nonlinear way as a function of EF for the M and Au−M−Au models; this result is taken into account as an index of the molecular response to EF of the distributions of the electric charges in the proposed molecular switch. Also, the direction of the applied field is clearly evident in the change in the dipole moment of the molecule. In addition, it is obtained that the atomic basins are found in the direction of application of the field, which is more significant than that of the other components of ($\mu i$). Note that the EF is applied along axes X and Y.

To evaluate the cause of the overpotential in the charging and current transfer processes of an electrode and to measure the sensitivity of the molecule to the EF, the electron spatial extent (ESE) has been defined as a principal parameter for this concept (see Figure 14). When the EF is applied along the X- and Y-axes, the ESE value shows a significant change in the field intensity of $80-60 \times 10^{-4}$ and $80-100 \times 10^{-4}$ a.u., respectively. It is predicted that when ESE increases, the ET efficiency (corresponding to local charge/energy transfer, secs 3−12) of the molecular switch increases.

It appears that at an important point when the field is applied along the X-axis, no significant change in the ESE value can be seen in the field intensity range of $0-60 \times 10^{-4}$ and $80-140 \times 10^{-4}$ a.u. Also, when the field is applied along the Y-axis, the ESE value does not change significantly in the field intensity range of $0 \times 10^{-4}$ to $80 \times 10^{-4}$ a.u. and $100 \times 10^{-4}$ to $140 \times 10^{-4}$ a.u.

The observed negligibly small changes in the electronic spatial extent under various EF strengths can be considered a positive index for this molecular switch in nanoelectronic circuits because of its negligible changes in the steric interaction with its neighboring nanoelectronic circuit components.

**3.11. Diagram and Switching Mechanism.** We calculated the $I-V$ curve of this molecular switch in both the M and Au−M−Au states using Landauer's formula (eq 6). Analysis of the obtained results revealed that the switching mechanism of this molecular switch occurs at an EF intensity higher than the threshold intensity ($\phi < \text{EF}$). The effect of the external EF on this molecular switch becomes evident when the field strength (intensity) reaches 0.008 au along the X-axis or 0.006 au along the Y-axis. In these cases, the molecular switch is turned ON, as shown in Figure 15a,b.
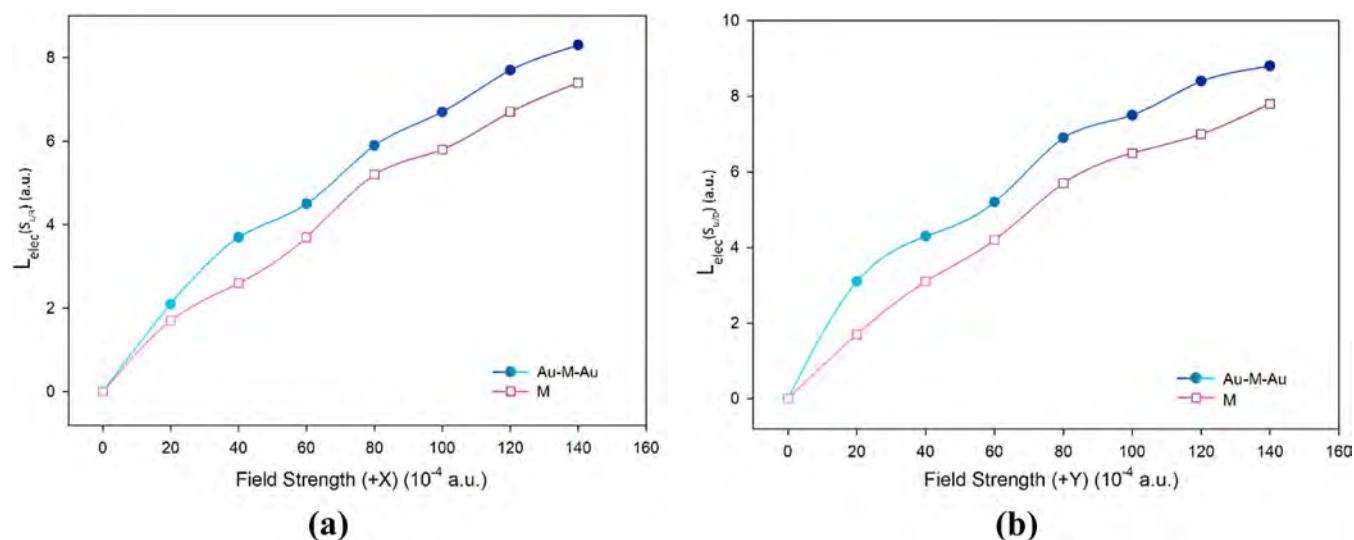
**Figure 18.** External EF effect [(a) along the *X*-axis and (b) along the *Y*-axis] on the electronic phenomenological coefficients, $L_{elec}$ ($S_{L/U}$,$S_{R/D}$) in M and Au−M−Au studied systems.

The switching process in a molecular switch can be controlled by external stimuli such as an external EF. As depicted in Figures S2−S4 and 8−13, the molecular and atomic electronic properties of this molecular switch exhibit significant dependence on both the field intensity and field direction. This characteristic highlights the observable and measurable response of the studied molecular switch to the applied field's properties, including field intensity and direction (*x* or *y*). These electronic changes suggest an increase in the distribution or redistribution of charge and energy transfer between different intramolecular sections (atomic basins) within the molecular switch, triggered by the applied external field. Furthermore, for planar molecular systems such as the one under investigation, charge and energy transfers primarily occur within the *x*−*y* plane, indicating that the switching mechanism is likely to be influenced when the field is applied in the *x* or *y* direction.

As illustrated in Figures 16 and 17, in a redox molecular switch system, the pathway of *π*-electron displacement plays a pivotal role in determining the switch's functionality. Additionally, the application of an external EF to a molecular switch can result in the separation of positive and negative charge centers within the structure, leading to changes in its electric dipole moments (as shown in Figure 13). These changes are associated with the expansion of the *π*-conjugation electron system along the molecule's length due to the external field, subsequently increasing molecular conductivity in the ON-circuit state. The increase in the molecular electrical conductivity (*G*) may also stem from a reduction in the HLG gap caused by the amplified intensity of externally applied fields (as depicted in Figures 7−15). Consequently, it is anticipated that structural-conformation changes will occur in this molecular switch due to the application of an external EF. These alterations in the electronic structure can influence the electron potential barrier and, thereby, affect molecular conductivity, ultimately affecting the switching mechanism.

**3.12. Local Electronic Intramolecular Phenomenological Coefficients: Onsager Phenomenological Approach (Linear Law).** It can be obtained through an exchange or a transfer of charge and energy between different atomic basins or different intramolecular systems (Sq) in the case where the

molecular device operating by the field effect is subjected to an external field (as shown in Figure 17a,b).

Moreover, it is clearly apparent that the investigated intramolecular charge-energy transfer and energy dissipation in single-molecular nanoelectronic systems are of specific importance. So far, many attempts have been made to understand thermal/electric (as thermoelectric) effects/phenomena in nanosized and molecular nanoelectronic systems.[56,57]

In this study, the local electronic intramolecular phenomenological coefficients, $L_{elec}$ ($S_{L/U}$, $S_{R/D}$), of the molecular switch studied in this work are calculated using the Onsager phenomenological approach. The Onsager phenomenological approach, also called the linear force-flux law, is expressed as follows

$$J_i = \sum_k L_{ik} \cdot X_k \tag{10}$$

where $J_i$, $K_k$, and $L_{ik}$ are fluxes, forces, and the phenomenological coefficients,[58−60] respectively.

Thus, $L^M$ can be introduced as

$$\nabla E = L^M \otimes F_{elec}, \begin{pmatrix} \nabla_x E \\ \nabla_y E \\ \nabla_z E \end{pmatrix} = \begin{pmatrix} L^M_{xx} & L^M_{xy} & L^M_{xz} \\ L^M_{yx} & L^M_{yy} & L^M_{yz} \\ L^M_{zx} & L^M_{zy} & L^M_{zz} \end{pmatrix} \begin{pmatrix} f_x \\ f_y \\ f_z \end{pmatrix} \tag{11}$$

where $\nabla_q E$ is the energy transferred between intramolecular sections (such as $S_L \leftrightarrow S_R$ or $S_U \leftrightarrow S_D$) due to the application of electric force $F_{elec}$.

In addition, using the AIM theory, the local (sectional) electronic kinetic energy can be defined as

$$K_{elec}(S_i, \varepsilon) = \sum_{\Omega \in S_i} K_{elec}(\Omega, \varepsilon), \qquad i \in \{R, L, U, D\} \tag{12}$$

Thus, the differential kinetic energy between intramolecular sections (such as $S_{L/U} \leftrightarrow S_{R/D}$) in the external EF of $\varepsilon$ intensity is given by

$$\begin{cases} \nabla_{x,\varepsilon} K_{\text{elec}} = K_{\text{elec}}(S_L, \varepsilon) - K_{\text{elec}}(S_R, \varepsilon) \\ \nabla_{,\varepsilon} K_\gamma = K_\gamma(S_U, \varepsilon) - K_\gamma(S_D, \varepsilon) \end{cases} \quad (13)$$

Also, the change in the local differential kinetic electronic energies is given by

$$\begin{cases} \Delta_{x,\varepsilon} = \nabla_{x,\varepsilon} K_{\text{elec}} - \nabla_{x,0} K_{\text{elec}} \\ \Delta_{y,\varepsilon} = \nabla_{y,\varepsilon} K_{\text{elec}} - \nabla_{y,0} K_{\text{elec}} \end{cases} \quad (14)$$

The local electronic phenomenological coefficient is developed based on the linear force-flux law as follows:

$L_{\text{elec}}$ $(S_{L/U}, S_{R/D})$ is given by

$$L_{\text{elec}}(S_L, S_R) = \frac{\nabla E(S_L, S_R)}{\varepsilon} \quad (15)$$

$$L_{\text{elec}}(S_U, S_D) = \frac{\nabla E(S_U, S_D)}{\varepsilon} \quad (16)$$

Based on[13−16], the electronic $L_{\text{elec}}$ $(S_{L/U}, S_{R/D})$ coefficients of M and Au−M−Au systems are calculated, and a sample of these results is shown in Figure 18a,b.

Figure 18 also shows that $L_{\text{elec}}$ $(S_{L/U}, S_{R/D})$ increases almost linearly with external field intensity. Thus, the value (and sign) of the electronic $L_{\text{elec}}$ $(S_{L/U}, S_{R/D})$ coefficients can correspond to local charge and energy transfer between the $(S_{L/U} \leftrightarrow S_{R/D}, S_R)$ intramolecular sections, as induced by an external EF (along the $x$ and $y$ directions).

It can also be predicted that the molecular electrical conductance $(G \propto 1/R)$ increases when $L_{\text{elec}}$ $(S_{L/U}, S_{R/D})$ increases. Also, it is predicted that, as a result of reversing the direction of the initial direct EF (such as $+x \rightarrow -x$), the value and sign of the intramolecular electron coefficients do not necessarily change inversely (compared to their initial value). This issue can indicate the anisotropy of these intramolecular electron coefficients [for example, $L_{\text{elec},+x}$ $(S_i, S_j) \neq -L_{\text{elec},-x}$ $(S_i, S_j)$].

## 4. CONCLUSIONS

In this study, we investigate the impact of EFs along the $X$- and $Y$-axes on the electronic and vibrational properties of a field-effect molecular switch, employing DFT and AIM theories. It is worth noting that we predict the electrical conductivity behavior $(I-V$ curve) of the studied models without the use of numerical methods like Green's function or GF methods, relying on the quantum information on the system.

The application of an external EF leads to atomic charge separation, changes in ESE, a reduction in the energy gap (HLG), and, as a result, an increase in the electrical conductivity of the molecular system under study. Furthermore, our analysis of the results indicates that the application of an external EF induces charge and energy exchange between various atomic substrates, thereby altering the kinetic and potential (virial) energies of the molecular system.

Furthermore, the impact of the EF on the studied molecular structure reveals that above $100 \times 10^{-4}$ au along the $X$-axis, the molecular switch turns ON, driven by the movement of $\pi$-paired electrons along the molecule's length. When applying the EF along the $Y$-axis, the switch turns ON as the field intensity increases to $80 \times 10^{-4}$ a.u. Additionally, the calculation of the electronic intramolecular phenomenological coefficients, $L_{\text{elec}}$, demonstrates an almost linear increase with rising external field intensity. The value and sign of these electronic coefficients, $L_{\text{elec}}$, are indicative of the mechanism of charge and energy transfer between different intramolecular sections.

## ■ ASSOCIATED CONTENT

### Data Availability Statement

All data are included in the manuscript.

### ⓢ Supporting Information

The Supporting Information is available free of charge at https://pubs.acs.org/doi/10.1021/acsomega.3c07257.

> Atomic electronic charges for certain atomic basins (M along the $X$- and $Y$-axes); representation of the electron density (RHO) for certain atomic basins for our isolated molecular switch (M along the $X$ and $Y$-axes) under the effect of an external field; effect of the EF (along the $X$- and $Y$-axes) on the length of the designed molecular switches; and effect of the EF (M along the $X$- and $Y$-axes) on the bond length of some important atomic basins in the isolated state molecular switch (M) (PDF)

## ■ AUTHOR INFORMATION

### Corresponding Author

**Sahbi Ayachi** − *Laboratory of Physico-Chemistry of Materials (LR01ES19), Faculty of Sciences, Avenue of the Environment, University of Monastir, Monastir 5019, Tunisia;* ⓞ orcid.org/0000-0003-1526-4298; Email: ayachi_sahbi@yahoo.fr

### Authors

**Hamid Hadi** − *Department of Chemistry, Physical Chemistry Group, Lorestan University, Khorramabad 6815144316, Iran*

**Bouzid Gassoumi** − *Laboratory of Advanced Materials and Interfaces (LIMA), Faculty of Sciences, Avenue of the Environment, University of Monastir, Monastir 5019, Tunisia*

**Samia Nasr** − *Department of Chemistry, Faculty of Science, King Khalid University, Abha 61413, Saudi Arabia*

**Reza Safari** − *Department of Chemistry, Physical Chemistry Group, University of Qom, Qom 3716146611, Iran*

**A. Aathif Basha** − *Department of Physics, Islamiah College (Autonomous), Vaniyambadi 635752, India;* ⓞ orcid.org/0000-0002-0415-327X

**Predhanekar Mohamed Imran** − *Department of Chemistry, Islamiah College (Autonomous), Vaniyambadi 635752, India*

**Houcine Ghalla** − *Quantum and Statistical Physics Laboratory, Faculty of Sciences, Avenue of the Environment, University of Monastir, Monastir 5019, Tunisia*

**Maria Teresa Caccamo** − *Dipartimento di Scienze Matematiche e Informatiche, Scienze Fisiche e Scienze della Terra, Università di Messina, Messina 98166, Italy*

Complete contact information is available at:
https://pubs.acs.org/10.1021/acsomega.3c07257

### Author Contributions

Hamid Hadi, Bouzid Gassoumi, and Sahbi Ayachi: conceptualization, methodology, writing—original draft, supervision, validation, and writing—review and editing. Samia Nasr, Reza Safari, and A. Aathif Basha: conceptualization, methodology, supervision, and review and editing. Predhanekar Mohamed Imran: conceptualization, methodology, and review of the manuscript. Houcine Ghalla and Maria Teresa Caccamo: supervision and review of the manuscript.

### Notes

The authors declare no competing financial interest.

## ■ REFERENCES

(1) Mathew, P. T.; Fang, F. Advances in Molecular Electronics: A Brief Review. *Engineering* **2018**, *4*, 760−771.

(2) Ratner, M. A brief history of molecular electronics. *Nat. Nanotechnol.* **2013**, *8*, 378−381.

(3) Heath, J. R.; Ratner, M. A. Molecular Electronics. *Phys. Today* **2003**, *56*, 43−49.

(4) Mostaanzadeh, H.; Safari, R.; Hadi, H.; Javadi, M. R. DFT Computational Study of a Candidate Field-Effect Molecular Wire. *Russ. J. Phys. Chem.* **2023**, *97*, 202−211.

(5) Li, T.; Bandari, V. K.; Schmidt, O. G. Molecular Electronics: Creating and Bridging Molecular Junctions and Promoting Its Commercialization. *Adv. Mater.* **2023**, *35*, 2209088.

(6) Tsutsui, M.; Taniguchi, M. Single Molecule Electronics and Devices. *Sensors* **2012**, *12*, 7259−7298.

(7) Quantum nanoscience, *Nat. Nanotechnol.* **2021**, *16*, 1293. .

(8) Weinbub, J.; Kosik, R. Computational perspective on recent advances in quantum electronics: from electron quantum optics to nanoelectronic devices and systems. *J. Phys.: Condens. Matter* **2022**, *34*, 163001.

(9) Zhao, Y.; Liu, W.; Zhao, J.; Wang, Y.; Zheng, J.; Liu, J.; Hong, W.; Tian, Z.-Q. The fabrication, characterization and functionalization in molecular electronics. *Int. J. Extrem. Manuf.* **2022**, *4*, 022003.

(10) Lan, Y.-K.; Yang, C. H.; Yang, H.-C. Theoretical investigations of electronic structure and charge transport properties in polythiophene-based organic field-effect transistors. *Polym. Int.* **2010**, *59*, 16−21.

(11) Safari, R.; Hadi, H.; Shamlouei, H. R. Quantum study of symmetrical/asymmetrical charge and energy transfer in a simple candidate molecular switch. *Struct. Chem.* **2023**, *34*, 59−70.

(12) Zhang, J. L.; Zhong, J. Q.; Lin, J. D.; Hu, W. P.; Wu, K.; Xu, G. Q.; Wee, A. T. S.; Chen, W. Towards single molecule switches. *Chem. Soc. Rev.* **2015**, *44*, 2998−3022.

(13) English, R. A.; Davison, S. G.; Miskovic, Z. L.; Goodman, F. O. Applied-field effects on molecular switches. *J. Phys.: Condens. Matter* **1998**, *10*, 4423−4434.

(14) Ke, G.; Duan, C.; Huang, F.; Guo, X. Electrical and spin switches in single-molecule junctions. *InfoMat* **2020**, *2*, 92−112.

(15) Li, H.; Qu, D.-H. Recent advances in new-type molecular switches. *China Chem.* **2015**, *58*, 916−921.

(16) Sabzyan, H.; Farmanzadeh, D. Electric field effects on the performance of a candidate multipole molecular switch: A quantum computational study. *J. Comput. Chem.* **2007**, *28*, 922−931.

(17) Hush, N. S.; Wong, A. T.; Bacskay, G. B.; Reimers, J. R. Electron and energy transfer through bridged systems. 6. Molecular switches: the critical field in electric field activated bistable molecules. *J. Am. Chem. Soc.* **1990**, *112*, 4192−4197.

(18) Otsuki, J.; Akasaka, T.; Araki, K. Molecular switches for electron and energy transfer processes based on metal complexes. *Coord. Chem. Rev.* **2008**, *252*, 32−56.

(19) *Nano and Molecular Electronics Handbook*; Routledge & CRC Press, 2023. https://www.routledge.com/Nano-and-Molecular-Electronics-Handbook/Lyshevski/p/book/9780849385285 (accessed Nov 3, 2023).

(20) Del Nero, J.; de Souza, F. M.; Capaz, R. B. Molecular Electronics Devices: A Short Review. *J. Comput. Theor. Nanosci.* **2010**, *7*, 503−516.

(21) Li, Y.; Xu, K.; Sun, X. Single molecule switch devices: A mini review. *Instrum. Sci. Technol.* **2020**, *48*, 518−538.

(22) Audi, H.; Viero, Y.; Alwhaibi, N.; Chen, Z.; Iazykov, M.; Heynderickx, A.; Xiao, F.; Guérin, D.; Krzeminski, C.; Grace, I. M.; Lambert, C. J.; Siri, O.; Vuillaume, D.; Lenfant, S.; Klein, H. Electrical molecular switch addressed by chemical stimuli. *Nanoscale* **2020**, *12*, 10127−10139.

(23) Somashekar, M. N.; Chetana, P. R. A Review on anthracene and its derivatives: applications. 2016, http://13.232.72.61:8080/jspui/handle/123456789/2025 (accessed Dec 3, 2023).

(24) Islam, K.; Bhunia, B. K.; Mandal, G.; Nag, B.; Jaiswal, C.; Mandal, B. B.; Kumar, A. Room-Temperature, Copper-Free, and Amine-Free Sonogashira Reaction in a Green Solvent: Synthesis of Tetraalkynylated Anthracenes and In Vitro Assessment of Their Cytotoxic Potentials. *ACS Omega* **2023**, *8*, 16907−16926.

(25) Yanai, T.; Tew, D. P.; Handy, N. C. A new hybrid exchange-correlation functional using the Coulomb-attenuating method (CAM-B3LYP). *Chem. Phys. Lett.* **2004**, *393*, 51−57.

(26) Chiodo, S.; Russo, N.; Sicilia, E. LANL2DZ basis sets recontracted in the framework of density functional theory. *J. Chem. Phys.* **2006**, *125*, 104107.

(27) Glasser, L.; Sheppard, D. A. Cohesive Energies and Enthalpies: Complexities. Confusions. and Corrections. *Inorg. Chem.* **2016**, *55*, 7103−7110.

(28) O'Boyle, N. M.; Tenderholt, A. L.; Langner, K. M. cclib: A library for package-independent computational chemistry algorithms. *J. Compd. Chem.* **2008**, *29*, 839−845.

(29) Sun, H.; Autschbach, J. Electronic Energy Gaps for π-Conjugated Oligomers and Polymers Calculated with Density Functional Theory. *J. Chem. Theory Comput.* **2014**, *10*, 1035−1047.

(30) Landauer, R. Electrical transport in open and closed systems. *Z. Physik B - Condensed Matter* **1987**, *68*, 217−228.

(31) Ando, T., Landauer's Formula. In *Mesoscopic Physics and Electronics*; Ando, T., Arakawa, Y., Furuya, K., Komiyama, S., Nakashima, H., Eds.; Springer: Berlin, Heidelberg, 1998; pp 11−14.

(32) Singh, U. C.; Kollman, P. A. An approach to computing electrostatic charges for molecules. *J. Comput. Chem.* **1984**, *5*, 129−145.

(33) Rizzo, R. C.; Jorgensen, W. L. OPLS All-Atom Model for Amines: Resolution of the Amine Hydration Problem. *J. Am. Chem. Soc.* **1999**, *121*, 4827−4836.

(34) Polanyi, M. "The electrostatic theory of adsorption and catalysis". *Trans. Faraday Soc.* **1933**, *29*, 431−438.

(35) Gohlke, H.; Klebe, G. Approaches to the Description and Prediction of the Binding Affinity of Small-Molecule Ligands to Macromolecular Receptors. *Angew. Chem., Int. Ed.* **2002**, *41*, 2644−2676.

(36) Shin, D.; Jung, Y. Molecular electrostatic potential as a general and versatile indicator for electronic substituent effects: statistical analysis and applications. *Phys. Chem. Chem. Phys.* **2022**, *24*, 25740−25752.

(37) Lakshminarayanan, S.; Jeyasingh, V.; Murugesan, K.; Selvapalam, N.; Dass, G. Molecular electrostatic potential (MEP) surface analysis of chemo sensors: An extra supporting hand for strength, selectivity & non-traditional interactions. *J. Photochem. Photobiol.* **2021**, *6*, 100022.

(38) Luque, F. J.; Orozco, M.; Illas, F.; Rubio, J. Effect of electron correlation on the electrostatic potential distribution of molecules. *J. Am. Chem. Soc.* **1991**, *113*, 5203−5211.

(39) Silvi, B.; Savin, A. Classification of chemical bonds based on topological analysis of electron localization functions. *Nature* **1994**, *371*, 683−686.

(40) Kulinich, A. V.; Ishchenko, A. A. Electronic structure of merocyanine dyes derived from 3H-indole and malononitrile in the ground and excited states: DFT/TD-DFT analysis. *Comput. Theor. Chem.* **2019**, *1154*, 50−56.

(41) Chérif, I.; Raissi, H.; Abiedh, K.; Gassoumi, B.; Teresa, C.; Magazu, S.; Said, A. H.; Hassen, F.; Boubaker, T.; Ayachi, S. Photophysical and nonlinear optical properties of para-substituted nitrobenzofurazan: A comprehensive DFT investigation. *J. Photochem. Photobiol., A* **2023**, *443*, 114850.

(42) Gassoumi, B.; Mehri, A.; Hammami, H.; Castro, M. E.; Karayel, A.; Özkınalı, S.; Melendez, F. J.; Nouar, L.; Madi, F.; Ghalla, H.;

Chaabane, R. B.; Ben Ouada, H. Spectroscopic characterization, host-guest charge transfer, Hirshfeld surfaces, AIM-RDG and ELF study of adsorption and chemical sensing of heavy metals with new derivative of Calix [4]quinone: A DFT-D3 computation. *Mater. Chem. Phys.* **2022**, *278*, 125555.

(43) Jiang, G.; Ma, Y.; Ding, J.; Liu, J.; Liu, R.; Zhou, P. N-Protonation as a Switch of the Twisted Excited States with $\pi\pi^*$ or $n\pi^*$ Character and Correlation with the $\pi$-Electrons Characteristic of Rotatable Bonds. *Chem. -Eur. J.* **2023**, *29* (38), No. e202300625.

(44) Rizwana, F.; Prasana, J. C.; Muthu, S.; Abraham, C. S. Molecular docking studies, charge transfer excitation and wave function analyses (ESP, ELF, LOL) on valacyclovir: A potential antiviral drug. *Comput. Biol. Chem.* **2019**, *78*, 9−17.

(45) Becke, A. D.; Edgecombe, K. E. A simple measure of electron localization in atomic and molecular systems. *J. Chem. Phys.* **1990**, *92*, 5397−5403.

(46) Gassoumi, B.; Ben Mohamed, F. E.; Castro, M. E.; Melendez, F. J.; Karayel, A.; Nouar, L.; Madi, F.; Ghalla, H.; Özkınalı, S.; Kovalenko, V. I.; Ben Chaabane, R.; Ben Ouada, H. In silico exploration of O-H. . .X2+ (X = Cu, Ag, Hg) interaction, targeted adsorption zone, charge density iso-surface, O-H proton analysis and topographic parameters theory for calix[6]arene and calix[8]arene as model. *J. Mol. Liq.* **2021**, *334*, 116127.

(47) Bader, R. F. W. A Bond Path: A Universal Indicator of Bonded Interactions. *J. Phys. Chem. A* **1998**, *102*, 7314−7323.

(48) Jeba Reeda, V. S.; Bena Jothy, V. Vibrational spectroscopic, quantum computational (DFT), reactivity (ELF, LOL and Fukui), molecular docking studies and molecular dynamic simulation on (6-methoxy-2-oxo-2H-chromen-4-yl) methyl morpholine-4-carbodi-thioate. *J. Mol. Liq.* **2023**, *371*, 121147.

(49) Pramila, M. J.; Dhas, D. A.; Joe, I. H.; Balachandran, S.; Vinitha, G. Structural insights, spectral, fluorescence, Z-scan, C-H. . .O/N-H. . .O hydrogen bonding and AIM, RDG, ELF, LOL, FUKUI analysis, NLO activity of N-2(Methoxy phenyl) acetamide. *J. Mol. Struct.* **2023**, *1272*, 134140.

(50) Sukanya, R.; Aruldhas, D.; Hubert Joe, I.; Balachandran, S. Spectroscopic and quantum chemical computation on molecular structure, AIM, ELF, RDG, NCI, and NLO activity of 4-VINYL benzoic acid: A DFT approach. *J. Mol. Struct.* **2022**, *1253*, 132273.

(51) Harzallah, M.; Medimagh, M.; Issaoui, N.; Roisnel, T.; Brahim, A. Synthesis, X-ray crystal structure, Hirshfeld surface analysis, DFT, AIM, ELF, RDG and molecular docking studies of bis[4-(dimethylamino)pyridinium]di-$\mu$-chlorido-bis[dichloridomercurate-(II)]. *J. Coord. Chem.* **2021**, *74*, 2927−2946.

(52) Sheena Mary, Y.; Shyma Mary, Y.; Serdaroglu, G.; Kaya, S.; Sarojini, B. K.; Umamahesvari, H.; Mohan, B. J. Conformational Analysis, Spectroscopic Insights, Chemical Descriptors, ELF, LOL and Molecular Docking Studies of Potential Pyrimidine Derivative with Biological Activities. *Polycyclic Aromat. Compd.* **2022**, *42*, 5160−5170.

(53) Choudhary, V.; Bhatt, A.; Dash, D.; Sharma, N. DFT calculations on molecular structures, HOMO-LUMO study, reactivity descriptors and spectral analyses of newly synthesized diorganotin(IV) 2-chloridophenylacetohydroxamate complexes. *J. Comput. Chem.* **2019**, *40*, 2354−2363.

(54) Joseph, S.; Thomas, S.; Mohan, J.; Kumar, A. S.; Jayasree, S. T.; Thomas, S.; Kalarikkal, N. Theoretical Study on Tuning Band Gap and Electronic Properties of Atomically Thin Nanostructured MoS2/Metal Cluster Heterostructures. *ACS Omega* **2021**, *6*, 6623−6628.

(55) Toriyama, M. Y.; Ganose, A. M.; Dylla, M.; Anand, S.; Park, J.; Brod, M. K.; Munro, J. M.; Persson, K. A.; Jain, A.; Snyder, G. J. How to analyse a density of states. *Materials Today Electron.* **2022**, *1*, 100002.

(56) Safari, R.; Sabzyan, H. Local Energy Dissipation/Transition in Field Effect Molecular Nanoelectronic Systems: a Quantum Mechanical Methodology. *Commun. Theor. Phys.* **2019**, *71*, 441.

(57) Naher, M.; Milan, D. C.; Al-Owaedi, O. A.; Planje, I. J.; Bock, S.; Hurtado-Gallego, J.; Bastante, P.; Abd Dawood, Z. M.; Rincón-García, L.; Rubio-Bollinger, G.; Higgins, S. J.; Agraït, N.; Lambert, C. J.; Nichols, R. J.; Low, P. J. Molecular Structure-(Thermo)electric Property Relationships in Single-Molecule Junctions and Comparisons with Single- and Multiple-Parameter Models. *J. Am. Chem. Soc.* **2021**, *143*, 3817−3829.

(58) Onsager, L. Reciprocal Relations in Irreversible Processes. II. *Phys. Rev.* **1931**, *38*, 2265−2279.

(59) Yao, Y. L. *Irreversible Thermodynamics*; Science Press: Beijing, 1981. (distributed by Van Norstrand Reinhold, NY).

(60) Sabzyan, H.; Safari, R. Intramolecular thermoelectric-like effects in field-effect molecular nanoelectronic devices. *Europhys. Lett.* **2012**, *99*, 67005.